

Probing $tt\gamma$ and ttZ couplings at the LHeC

Antonio O. Bouzas and F. Larios*

Departamento de Física Aplicada, CINVESTAV-Mérida,

A.P. 73, 97310 Mérida, Yucatán, México

We study the deep inelastic scattering and photo-production modes of $t\bar{t}$ pairs at the proposed LHeC and its potential to probe the electromagnetic and weak dipole moments (MDM and EDM for $tt\gamma$) of the top quark. A framework of eight independent gauge-invariant dimension-six operators involving the top quark and the electroweak gauge bosons is used. Four of these operators modify the charged tbW coupling which can be probed through the single (anti) top production mode as reported in the literature. One generates $tt\gamma(Z)$ as well as tbW couplings, while the other two do not generate tbW but only $tt\gamma(Z)$. Our focus is on the MDM and EDM of the top quark for which the photo-production mode of $t\bar{t}$ can be an excellent probe. At the proposed electron energies of $E_e = 60$ and 140 GeV the LHeC could set constraints stronger than the indirect limits from $b \rightarrow s\gamma$ and the potential limits of the LHC through $t\bar{t}\gamma$ production.

PACS numbers: 14.65.Ha, 12.15.-y

* Corresponding author: larios@mda.cinvestav.mx.

I. INTRODUCTION

The Large Hadron Electron Collider (LHeC) is the proposal of a new electron beam with an energy $E_e = 60$ GeV, or possibly $E_e = 140$ GeV, to collide with one of the 7 TeV LHC proton beams at the high-luminosity phase [1]. Such a facility will be very useful in understanding parton and gluon interactions at very low x and very high Q^2 , thus providing a much needed complementary information to the physics program of the LHC. Moreover, the energy available will be enough to produce the two heaviest known particles: Higgs bosons and top quarks. Even though the cross sections are not as high as in the LHC, the cleaner environment will make this machine a good place to study the physics associated with these particles.

In this work we focus on top-quark production and on the potential of this machine to study the anomalous top-gauge boson couplings. In particular, for the case of the charged tbW effective vertex a recent study has shown that the LHeC sensitivity will surpass that achievable at the LHC [2]. Here, we want to consider the neutral $tt\gamma$ and ttZ vertices and find out if the sensitivity of the LHeC is better than that of the LHC for these couplings as well.

The top-quark couplings with the gauge bosons can be modified significantly in models with new top (or third generation) partners. This is the case of some extensions of the minimal supersymmetric standard model [3, 4], in little Higgs models [5], top-color models [6], top seesaw [7], top compositeness [8], and others. Testing them is therefore of paramount importance to find out whether there are other sources of electroweak symmetry breaking that are different from the standard Higgs mechanism.

In this paper we concentrate on the two possible values of the electron energy, $E_e = 60, 140$ GeV, as is planned. Concerning the potential luminosity, since it is proposed that the LHeC will run simultaneously with the high-luminosity period of the LHC14 (sometime around 2024), it is believed that an integrated luminosity of order 100 fb^{-1} is achievable [1]. For this luminosity, and for $E_e = 60$ (140) GeV, the LHeC will yield about 2 (6) $\times 10^5$ single top events as well as 4 (23) $\times 10^3$ $t\bar{t}$ events. The high rate for single top events along with a cleaner environment makes the LHeC a much better place to probe the tbW coupling than the LHC [2]. As we shall see below, for the case of $t\bar{t}$ production, even though the rate is about one order of magnitude lower, the potential for measuring the $tt\gamma$ magnetic and electric dipole

moments (MDM and EDM, respectively) is also better than at the LHC14. The reason for this is that in $t\bar{t}$ photo-production the highly energetic incoming photon couples only to the t quark so that the cross section depends directly on the $tt\gamma$ vertex. In contrast, at the LHC the way to probe the $tt\gamma$ vertex is through $t\bar{t}\gamma$ production, and in this case the outgoing photon could come from other charged sources, like the top decay products. The deep inelastic scattering (DIS) regime of $t\bar{t}$ production will also be able to probe the ttZ coupling, albeit with less sensitivity. In the framework of the effective Lagrangian with $SU(2) \times U(1)$ gauge-invariant operators, some of the ttZ couplings are generated by the same operators that give rise to tbW and $tt\gamma$. This correlation could be used to accomplish a complete and very sensitive analysis of tbW , $tt\gamma$ and ttZ couplings at the LHeC.

The structure of this paper is as follows. In Sec. II we write down the eight independent dimension-six gauge-invariant operators that involve the top quark and the gauge bosons. Two of them generate the MDM and the EDM of the top quark and will be the focus of our study. A third operator that generates an anomalous $t_R t_R Z$ coupling can also be probed through the DIS mode of $t\bar{t}$ production. In Sec. III we review the standard model (SM) prediction for the most important modes of top-quark production at the LHeC. In Sec. IV we study the contributions of the anomalous dipole moments to $t\bar{t}$ photo-production. In Sec. V we consider the contribution of the three operators to DIS production of $t\bar{t}$. Assuming an integrated luminosity of 100 fb^{-1} , we estimate the expected number of events that will meet the experimental conditions for detection. From there, we present the estimated sensitivities.

II. DIMENSION-SIX $SU(2) \times U(1)$ EFFECTIVE OPERATORS

The SM, based on the $SU(3) \times SU(2)_L \times U(1)_Y$ gauge group, has been successful in describing essentially all the experimental observations at SLAC, LEP, the Tevatron, the LHC, and other colliders. Moreover, the discovery of what appears to be the Higgs boson at the LHC seems to indicate that the Higgs mechanism is indeed the explanation for the electroweak symmetry breaking. However, the SM is believed to be an effective theory that is valid below a certain scale Λ . At and above this scale the heavy degrees of freedom of a larger theory become apparent. Therefore, it has been proposed that new physics effects may be properly described by an effective Lagrangian that contains the SM dimension-four

gauge-invariant operators plus higher-dimensional ones that are suppressed by powers of Λ ,

$$\mathcal{L} = \mathcal{L}_{\text{SM}} + \frac{1}{\Lambda^2} \sum_k \left(C_k O_k^{(6)} + \text{h.c.} \right) + \dots .$$

About 30 years ago Buchmueller and Wyler presented a long list of gauge-invariant operators that were supposed to be independent [9]. Some years later it was shown that some of the operators involving the top quark were in fact redundant [10]. Then, after a thorough analysis made in Ref. [11], a reduced list of only eight operators involving the top quark and the gauge bosons was presented. Recently, a revised general list of all gauge-invariant operators—including those in [11] and others not necessarily related to the top quark—was given in Ref. [12]. Naturally, one could think of a different set of independent operators that should be equivalent to the ones presented in Refs. [11, 12]. In any case, it has been pointed out that this list in particular satisfies a so-called criterion of Potential-Tree-Generated operators, which means that they may have the largest possible coefficients [13].

The minimal nonredundant set of dimension-six gauge-invariant operators that give rise to effective top-quark vertices with the gauge bosons is [11]:

$$\begin{aligned} O_{\phi q}^{(3,ij)} &= i\phi^\dagger \tau^I D_\mu \phi \bar{q}_{Li} \gamma^\mu \tau^I q_{Lj}, & O_{uW}^{ij} &= \bar{q}_{Li} \sigma^{\mu\nu} \tau^I u_{Rj} \tilde{\phi} W_{\mu\nu}^I, \\ O_{\phi q}^{(1,ij)} &= i\phi^\dagger D_\mu \phi \bar{q}_{Li} \gamma^\mu q_{Lj}, & O_{dW}^{ij} &= \bar{q}_{Li} \sigma^{\mu\nu} \tau^I d_{Rj} \phi W_{\mu\nu}^I, \\ O_{\phi u}^{ij} &= i\phi^\dagger D_\mu \phi \bar{u}_{Ri} \gamma^\mu u_{Rj}, & O_{uB\phi}^{ij} &= \bar{q}_{Li} \sigma^{\mu\nu} u_{Rj} \tilde{\phi} B_{\mu\nu}, \\ O_{\phi\phi}^{ij} &= i\tilde{\phi}^\dagger D_\mu \phi \bar{u}_{Ri} \gamma^\mu d_{Rj}, & O_{uG\phi}^{ij} &= \bar{q}_{Li} \lambda^a \sigma^{\mu\nu} u_{Rj} \tilde{\phi} G_{\mu\nu}^a. \end{aligned} \quad (1)$$

Notice that every operator actually defines three or more variations depending on the flavor content. However, in this study we will not consider effects from flavor-changing operators. Each operator is multiplied by a term $\Lambda^{-2} C_k^{ij}$, with Λ being the scale below which the effective gauge-invariant Lagrangian is valid, and C_k^{ij} a complex parameter. For concreteness we set $\Lambda \equiv 1$ TeV, but we can go back to a general Λ by just replacing C_k^{ij} by C_k^{ij}/Λ^2 . Thus, dimensionful parameters in the operators should be given in units of TeV, like $v = 0.246$, $m_t = 0.173$ and $m_W = 0.08$. We use standard notation in Eq. (1), with I, J, K SU(2) being gauge indices, τ^I the Pauli matrices, q_{Li} the left-handed quark doublet, u_{Rj} the right-handed up-quark singlet, and ϕ the SM Higgs doublet with $\tilde{\phi} = i\tau^2 \phi^*$ and, in unitary gauge, $\phi = (0, v + h)$. Also, $W_{\mu\nu}^I = \partial_\mu W_\nu^I - \partial_\nu W_\mu^I + g\epsilon_{IJK} W_\mu^J W_\nu^K$ and $B_{\mu\nu} = \partial_\mu B_\nu - \partial_\nu B_\mu$ are the SU(2)_L and U(1)_Y field strength tensors, respectively. In addition, for the operators on the left column $D_\mu = \partial_\mu - ig\frac{1}{2}\tau^I W_\mu^I - ig'\frac{1}{2}B_\mu$ is the Higgs field covariant derivative [38].

For each pair i, j of flavor indices there are eight operators in Eq. (1), seven of which involve the electroweak gauge bosons and one involves the gluon field. In this paper we focus on the flavor-diagonal $ij = 33$ operators [39]. The associated coefficients C_k^{33} are in general complex: their real and imaginary parts will give rise to CP -even and CP -odd couplings, respectively. In Table I we show explicitly the top–gauge boson vertices coming from each operator, with the Higgs doublet substituted by its vacuum expectation value v plus the neutral scalar field h . Notice that the CP -odd parts of the operators $O_{\phi q}^{(3,33)}$, $O_{\phi q}^{(1,33)}$, and $O_{\phi u}^{33}$ are not listed since, as shown in Ref. [15], the combinations $O_k^{ij} - O_k^{ij\dagger}$ of these operators are actually redundant and can be dropped from the operator list. Therefore, the coefficients $C_{\phi q}^{(3,33)}$, $C_{\phi q}^{(1,33)}$, and $C_{\phi u}$ must be real numbers. For the remaining coupling constants in Table I, which are complex, we introduce for simplicity the notation $C_k \equiv C_k^r + iC_k^i$.

Besides the vertices involving the top quark shown in Table I, some flavor-diagonal operators also generate vertices with only the bottom quark. Three operators, $O_{\phi q}^{(3,33)}$, $O_{\phi q}^{(1,33)}$, and O_{dW}^{33} give rise to $\bar{b}bZ$ vertices among which, in particular, there is a deviation of the $b_L b_L Z$ coupling that is proportional to $C_{\phi q}^{(3,33)} + C_{\phi q}^{(1,33)}$. It is well known, however, that the left-handed bottom- Z coupling has been probed with great precision. In Ref. [16] a global analysis of the contributions of these operators to all major precision electroweak observables was made, where it was found that $C_{\phi q}^{(3,33)} + C_{\phi q}^{(1,33)}$ is bound to be 0.016 ± 0.021 (with $\Lambda \equiv 1\text{TeV}$). We will take advantage of this constraint to make the assumption [17]

$$C_{\phi q}^{(3,33)} = -C_{\phi q}^{(1,33)} \equiv C_{\phi q}.$$

To simplify our notation, we will redefine our coefficients as $C_{\phi q}$, $C_{\phi t}$, $C_{\phi\phi}$, C_{tW} , C_{bW} and C_{tB} , as shown in Table I. Constraints from electroweak data and $b \rightarrow s\gamma$ observables can be found in Table II. These constraints were found by taking into account only one operator at a time, but in general there is a correlation between the coefficients [16, 18, 19].

Concerning the top-gluon operator $O_{uG\phi}^{33}$, it will be better probed at the LHC through the dominant $gg \rightarrow t\bar{t}$ process. Indeed, bounds of order 10^{-1} for $C_{uG\phi}^{33}$ have been obtained from the 7 TeV run of the LHC [23, 24] (see Table II), and they could be reduced further to a 10^{-2} level with the 14 TeV run. We have made an estimate of the sensitivity of $t\bar{t}$ production at the LHeC to the top-gluon couplings, and we obtain constraints that could be as low as 0.3 assuming an error of 10% in the measured cross section and taking only one anomalous coupling at a time. By the time the LHeC makes such measurements, the LHC data could

have already probed these couplings for values smaller by one order of magnitude. For that reason, we will not consider the anomalous top-gluon couplings further in this study.

As is common practice in the literature, we can write down the effective $tt\gamma$, ttZ and tbW couplings in terms of form factors:

$$\begin{aligned}
\mathcal{L}_{t\bar{t}\gamma} &= \frac{g}{\sqrt{2}}\bar{t}\left(\gamma^\mu W_\mu^+(F_1^L P_L + F_1^R P_R) - \frac{1}{2m_W}\sigma^{\mu\nu}W_{\mu\nu}^+(F_2^L P_L + F_2^R P_R)\right)b, \\
&+ e\bar{t}\left(Q_t\gamma^\mu A_\mu + \frac{1}{4m_t}\sigma^{\mu\nu}F_{\mu\nu}(\kappa + i\tilde{\kappa}\gamma_5)\right)t \\
&+ \frac{g}{2c_W}\bar{t}\gamma^\mu Z_\mu\left(\left(1 - \frac{4}{3}s_W^2 + F_{1Z}^L\right)P_L + \left(-\frac{4}{3}s_W^2 + F_{1Z}^R\right)P_R\right)t \\
&+ \frac{g}{2c_W}\bar{t}\left(\frac{1}{4m_t}\sigma^{\mu\nu}Z_{\mu\nu}(\kappa_Z + i\tilde{\kappa}_Z\gamma_5)\right)t
\end{aligned} \tag{2}$$

The relation between the form factors and the operator coefficients C_x^r is given by:

$$\begin{aligned}
F_1^L &= V_{tb} + \frac{v^2}{\Lambda^2}C_{\phi q}, & F_1^R &= \frac{1}{2}\frac{v^2}{\Lambda^2}C_{\phi\phi}^r, \\
F_2^L &= -\sqrt{2}\frac{v^2}{\Lambda^2}C_{tW}^r, & F_2^R &= -\sqrt{2}\frac{v^2}{\Lambda^2}C_{bW}^r, \\
F_{1Z}^L &= \frac{v^2}{\Lambda^2}C_{\phi q}, & F_{1Z}^R &= \frac{1}{2}\frac{v^2}{\Lambda^2}C_{\phi t}, \\
\kappa &= \frac{2\sqrt{2}vm_t}{e}\frac{1}{\Lambda^2}(s_W C_{tW}^r + c_W C_{tB}^r), & \kappa_Z &= \frac{4\sqrt{2}vm_t}{e}\frac{1}{\Lambda^2}s_W c_W (c_W C_{tW}^r - s_W C_{tB}^r).
\end{aligned} \tag{3}$$

The imaginary parts of the coefficients generate CP -odd interactions. For instance, the expressions for $\tilde{\kappa}$ and $\tilde{\kappa}_Z$ are the same as in Eq. (3) but with C_{tW}^r and C_{tB}^r replaced by C_{tW}^i and C_{tB}^i . Our main interests here are the anomalous MDM and EDM of the top quark, κ and $\tilde{\kappa}$, respectively. Comparing with other definitions we obtain the following relations:

$$\begin{aligned}
\kappa &= -F_{2V}^\gamma = \frac{2m_t}{e}\mu_t = Q_t a_t, \\
\tilde{\kappa} &= F_{2A}^\gamma = \frac{2m_t}{e}d_t,
\end{aligned} \tag{4}$$

where $a_t = (g_t - 2)/2$ is the anomalous MDM in terms of the gyromagnetic factor g_t . The factors F_{2V}^γ and F_{2A}^γ are used in Ref. [25]. Recent constraints coming from the branching ratio and a CP asymmetry for $b \rightarrow s\gamma$ can be found in Ref. [19]: $-2.0 < \kappa < 0.3$ and $-0.5 < \tilde{\kappa} < 1.5$.

Operator	Coefficient	CP -even ($O_x^{33} + O_x^{33\dagger}$)	CP -odd ($i(O_x^{33} - O_x^{33\dagger})$)
$(tb)O_{\phi q}^{(3,33)}$	$C_{\phi q}$	$\frac{g}{\sqrt{2}}\phi_0^2 (W_\mu^+ \bar{t}_L \gamma^\mu b_L + h.c.)$	---
$O_{\phi\phi}^{33}$	$C_{\phi\phi}$	$\frac{g}{2\sqrt{2}}\phi_0^2 (W_\mu^+ \bar{t}_R \gamma^\mu b_R + h.c.)$	$i\frac{g}{2\sqrt{2}}\phi_0^2 (W_\mu^+ \bar{t}_R \gamma^\mu b_R - h.c.)$
$(tb) O_{uW}^{33}$	C_{tW}	$2\phi_0 [D_{\mu\nu}^- \bar{b}_L \sigma^{\mu\nu} t_R + D_{\mu\nu}^+ \bar{t}_R \sigma^{\mu\nu} b_L]$	$i2\phi_0 [D_{\mu\nu}^- \bar{b}_L \sigma^{\mu\nu} t_R - D_{\mu\nu}^+ \bar{t}_R \sigma^{\mu\nu} b_L]$
O_{dW}^{33}	C_{bW}	$2\phi_0 [D_{\mu\nu}^+ \bar{t}_L \sigma^{\mu\nu} b_R + D_{\mu\nu}^- \bar{b}_R \sigma^{\mu\nu} t_L]$	$i2\phi_0 [D_{\mu\nu}^+ \bar{t}_L \sigma^{\mu\nu} b_R - D_{\mu\nu}^- \bar{b}_R \sigma^{\mu\nu} t_L]$
$(tt)O_{\phi q}^{(3,33)}$	$C_{\phi q}$	$\frac{g}{2c_w}\phi_0^2 \bar{t}_L \gamma^\mu t_L Z_\mu$	---
$O_{\phi q}^{(1,33)}$	$-C_{\phi q}$	$-\frac{g}{2c_w}\phi_0^2 \bar{t}_L \gamma^\mu t_L Z_\mu$	---
$O_{\phi u}^{33}$	$C_{\phi t}$	$-\frac{g}{2c_w}\phi_0^2 \bar{t}_R \gamma^\mu t_R Z_\mu$	---
$(tt) O_{uW}^{33}$	C_{tW}	$\sqrt{2}\phi_0 D_{\mu\nu}^3 \bar{t} \sigma^{\mu\nu} t$	$i\sqrt{2}\phi_0 D_{\mu\nu}^3 \bar{t} \sigma^{\mu\nu} \gamma_5 t$
$O_{uB\phi}^{33}$	C_{tB}	$\frac{1}{\sqrt{2}}\phi_0 B_{\mu\nu} \bar{t} \sigma^{\mu\nu} t$	$i\frac{1}{\sqrt{2}}\phi_0 B_{\mu\nu} \bar{t} \sigma^{\mu\nu} \gamma_5 t$
$O_{uG\phi}^{33}$	$C_{uG\phi}^{33}$	$\frac{1}{\sqrt{2}}\phi_0 \bar{t} \sigma^{\mu\nu} \lambda^a G_{\mu\nu}^a t$	$i\frac{1}{\sqrt{2}}\phi_0 \bar{t} \sigma^{\mu\nu} \gamma_5 \lambda^a G_{\mu\nu}^a t$

TABLE I: Diagonal operators with CP -even and CP -odd parts written separately. For $O_{\phi q}^{(1,33)}$, $O_{\phi q}^{(3,33)}$, and O_{dW}^{33} only the terms that involve the top quark are shown. We define $\phi_0 = v + h$, $D_{\mu\nu}^\pm = \partial_\mu W_\nu^\pm \pm igW_\mu^\pm W_\nu^3$, and $D_{\mu\nu}^3 = \partial_\mu W_\nu^3 - igW_\mu^+ W_\nu^-$. The real (imaginary) part of each coefficient multiplies the CP -even (odd) part of the corresponding operator (the scale factor Λ^{-2} is taken as 1 TeV^{-2}).

III. TOP-QUARK PRODUCTION AT THE LHeC

The most important top-production processes at the LHeC are single top, $t\bar{t}$, and associated tW production. In Table III we show the values of the associated cross sections for three electron energies. As seen there, the main source of production is single top via the charged current t channel [26] (see Fig. 1), whereas for the other modes, $t\bar{t}$ and tW , there is a lower though still sizeable production cross section. Given the advantage of an experimental environment cleaner than the LHC, we can envisage a good performance of this machine to do top-quark physics.

In this study we focus on the effective $t\bar{t}\gamma$ and $t\bar{t}Z$ couplings, and how they can be successfully tested at the LHeC. In this case the production mode to consider is that of $t\bar{t}$ for which the effects of these couplings, noticeably the electromagnetic dipole moments, on the cross section are significant. For $E_e = 60 \text{ GeV}$ we obtain for the photo-production (PHP) process (with $|Q_\gamma^2| < 2 \text{ GeV}^2$) $\sigma^{\text{SM}}(e(\gamma)p \rightarrow t\bar{t}) \simeq 0.023 \text{ pb}$, and for the DIS process

Operator	Indirect	LHC (7,8 TeV)
$O_{\phi q}^{(3,33)}$	$-0.35 < C_{\phi q} < 2.35$	$-2.1 < C_{\phi q} < 6.7$
$O_{\phi\phi}^{33}$	$0.004 < C_{\phi\phi}^r < 0.056$	$-6.6 < C_{\phi\phi}^r < 7.6$
$O_{\phi u}^{33}$	$-0.1 < C_{\phi t} < 3.7$	
O_{uW}^{33}	$-1.6 < C_{tW}^r < 0.8$	$-1.0 < C_{tW}^r < 0.5$
O_{dW}^{33}	$-0.01 < C_{bW}^r < 0.004$	$-1.7 < C_{bW}^r < 1.3$
$O_{uB\phi}^{33}$	$-6.0 < C_{tB}^r < 0.9$	
$O_{uG\phi}^{33}$	$-0.1 < C_{uG\phi}^r < 0.03$	$-0.3 < C_{uG\phi}^r < 0.06$

TABLE II: Current bounds on the coefficients (real part). The indirect bounds for the first four coefficients are taken from electroweak data [16], whereas the last three— C_{bW}^r [18], C_{tB}^r [19], and $C_{uG\phi}^r$ [20]—are taken from $b \rightarrow s\gamma$ measurements. Direct bounds come from measurements on the W helicity in top decays as well as single top production [21, 22].

Process	$E_e = 60\text{GeV}$	$E_e = 140\text{GeV}$	$E_e = 300\text{GeV}$
$ep(b) \rightarrow \nu\bar{t}$	2.0	5.9	13.0
$e(\gamma)p(g) \rightarrow t\bar{t}$	0.023	0.12	0.38
$ep(g) \rightarrow et\bar{t}$	0.020	0.11	0.34
$e(\gamma)p(b) \rightarrow \bar{t}W^+ + tW^-$	0.031	0.143	0.434
$ep(b) \rightarrow e\bar{t}W^+ + etW^-$	0.021	0.099	0.30
$\gamma p(g) \rightarrow t\bar{t}$	0.7	3.2	9.0

TABLE III: The SM cross sections (pb) for single antitop, $t\bar{t}$, and associated tW^- (or $\bar{t}W^+$) production processes at the LHeC. The bottom row shows $t\bar{t}$ production at an LHeC-based γp collider.

(with $|Q_\gamma^2| > 2\text{GeV}^2$) $\sigma^{\text{SM}}(ep \rightarrow t\bar{t}) \simeq 0.02$ pb (see Table III). At $E_e = 140$ GeV the cross sections grow by roughly a factor of 5 to 0.12 pb for PHP and 0.11 pb for DIS [1]. In this case the DIS mode could also be used to probe the $t\bar{t}Z$ couplings. We notice that, as shown at the bottom of Table III, the $\gamma p \rightarrow t\bar{t}$ production process at an LHeC-based γp collider reaches a value of $\sigma = 0.7$ pb for $E_e = 60$ GeV. The obvious conclusion is that in this case the $t\bar{t}\gamma$ (and maybe even the $t\bar{t}g$) coupling could be probed with remarkable sensitivity.

A less important production mode is $\bar{t}\gamma$ which, with the cut $p_T^\gamma > 10$ GeV, has a large enough cross section ~ 0.08 pb at $E_e = 140$ GeV. Thus, we could in principle consider it as another potential probe of the $t\bar{t}\gamma$ effective vertex. However, in this case photon emission originates in many sources other than the top quark: initial-state radiation, \bar{t} decay products and the virtual W boson, which will swamp the signal coming from the top-quark lines. The strong cuts needed to attain good sensitivity (see Ref. [19] for a similar analysis in the context of the LHC) would lead to unacceptably low cross sections. We therefore do not think this production mode could be very helpful. We do not consider other associated production modes, like $\bar{t}Z$ and $\bar{t}h$, which have cross sections smaller than 10 fb at $E_e = 140$ GeV (and probably $\lesssim 1$ fb after cuts are applied). If observable at all, they would be afflicted by excessively large experimental uncertainties.

Our analysis of the LHeC sensitivity to the $t\bar{t}\gamma$ and $t\bar{t}Z$ couplings is based solely on the measurement of the production cross section for $t\bar{t}$. With an integrated luminosity of 100 fb⁻¹, these cross sections translate to about 2300 PHP and 2000 DIS events at $E_e = 60$ GeV, and five times more at $E_e = 140$ GeV. As discussed in more detail in Sec. IV below, however, applying cuts to remove the background results in a substantial reduction of the signal. Thus, we expect statistical errors of $\sim 8\%$ at $E_e = 60$ GeV and $\sim 4\%$ at $E_e = 140$ GeV. Furthermore, we assume somewhat conservatively that systematical uncertainties will be about $\sim 10\%$ (see Sec. IV A below). Based on these experimental error estimates, we obtain remarkably tight bounds for the effective $t\bar{t}\gamma$ coupling. This is due to the fact that $t\bar{t}$ PHP in particular is naturally a direct probe of this coupling, which provides a remarkable enhancement of the sensitivity. We also obtain looser—but still interesting—bounds for the effective $t\bar{t}Z$ vertex.

We turn next to the dependence of the cross section on the effective couplings, by taking the contributions from the gauge-invariant operators one at a time. The production cross section at any given electron energy E_e depends quadratically on the effective couplings. For example, at $E_e = 60$ GeV the numerical expression for the contribution from the operator $O_{uB\phi}^{33}$ to the PHP cross section is found to be

$$\sigma(e(\gamma)p(g) \rightarrow t\bar{t})(\text{pb}) = 0.0228 - 0.0168C_{tB}^r + 0.0058|C_{tB}|^2,$$

where the scale $\Lambda \equiv 1$ TeV and the units are in pb. There can be no linear term in C_{tB}^i , since the anti-Hermitian part of $O_{uB\phi}^{33}$ is CP -odd and therefore cannot interfere with the

CP -even SM contribution. We can estimate the sensitivity to C_{tB} by assuming that the cross section measured at the LHeC is consistent with the SM prediction within a certain error. It is convenient to define the variation from the SM prediction as

$$R \equiv \frac{\sigma - \sigma_{\text{SM}}}{\sigma_{\text{SM}}} = aC_{tB}^r + b|C_{tB}|^2. \quad (5)$$

The above equation does not depend on the units of σ and, as it turns out, the numbers $a = -0.737$ and $b = 0.256$ do not change significantly at higher electron energies. Thus the sensitivity depends on the measurement error, but is largely independent of E_e in the range 60–300 GeV. Of course, at higher energies data samples will be larger and statistical errors correspondingly smaller. For the sake of concreteness, let us assume that with an integrated luminosity of 100 fb^{-1} the cross section for PHP of $t\bar{t}$ at $E_e = 60$ GeV is measured with an experimental error of 18%, whose plausibility we argue in Sec. IV. In order to obtain bounds on C_{tB} at the 1σ level we impose $R \leq \epsilon \equiv 0.18$ and find the limits from Eq. (5): $-0.23 < C_{tB}^r < 0.28$ and $|C_{tB}^i| < 0.81$.

From the point of view of the coupling of neutral currents to the top quark, three other operators besides $O_{uB\phi}^{33}$ are also potentially interesting. Together with $O_{uB\phi}^{33}$, $O_{\phi u}^{33}$ also generates $t\bar{t}Z$ but no tbW couplings, whereas $O_{\phi q}^{(3,33)}$ and O_{uW}^{33} generate $t\bar{t}\gamma(Z)$ as well as tbW couplings. The MDM κ and the EDM $\tilde{\kappa}$ are generated by $O_{uB\phi}^{33}$ as well as by O_{uW}^{33} . Since the focus of our study are the MDM and the EDM of the top quark, we will be mostly interested in these two operators. In numerical terms we obtain for the coefficients of interest (with $\Lambda \equiv 1 \text{ TeV}$)

$$\kappa = 0.185C_{tW}^r + 0.337C_{tB}^r, \quad \kappa_Z = 0.283C_{tW}^r - 0.155C_{tB}^r, \quad F_{RZ}^1 = 0.03C_{\phi t}. \quad (6)$$

Thus, from the bounds obtained above for C_{tB}^r and setting C_{tW}^r to zero in this equation, we get $-0.078 \leq \kappa \leq 0.094$. This is much more stringent than the limits $-0.8 \leq \kappa \leq 0.3$ obtained from $b \rightarrow s\gamma$ and a potential future measurement of $t\bar{t}\gamma$ at the LHC14 [19]. Similarly, we can obtain bounds for the other couplings as we did above for C_{tB} . We find essentially no sensitivity to the coupling $C_{\phi q}$ which, for this reason, we will not consider further. Assuming an experimental error of 18% we get, in PHP at $E_e = 60$ or 140 GeV, $-0.42 < C_{tW}^r < 0.51$, $|C_{tW}^i| < 1.5$. The anomalous ttZ coupling $C_{\phi t}$ contributes only to DIS, though with rather low sensitivity. Assuming an experimental error of 10% we obtain $-8 < C_{\phi t} < 12$.

For our calculations we used the program MADGRAPH 5 [27] with the parton distribution function (PDF) CTEQ6m [28] and the dynamic factorization and renormalization scales $\mu_f = \sqrt{4m_t^2 + \sum_i |\vec{p}_T(i)|^2} = \mu_r$, where the sum extends to all particles in the final state. To make a cross-check of some of our results we used CALCHEP 3.4 [29].

The results overviewed in this section were obtained from the amplitudes for the $t\bar{t}$ final state. In the following sections we present a more realistic and technically more detailed analysis based on the complete final partonic state.

IV. LIMITS FROM $t\bar{t}$ PHOTO-PRODUCTION.

In this section we make a more realistic analysis of $t\bar{t}$ photo-production by considering the complete process involving the final partonic state. Since t decays almost exclusively to Wb , $t\bar{t}$ production is observed in channels defined by the W decay modes. The branching fractions for W decay are 21.32% for light leptonic decays $\ell\nu$ ($\ell = e, \mu$), 11.25% for $\tau\nu$ decays, and 67.6% for hadronic decays to qq' [30]. Thus, for $t\bar{t}$ production followed by bW decays we have the branching fractions given in Table IV. The dominant modes are the hadronic ($jjjj$) and the semileptonic (ℓjj).

$\ell\ell$	$\tau\tau$	$jjjj$	$\ell\tau$	ℓjj	τjj
4.55%	1.27%	45.70%	4.80%	28.82%	15.2%

TABLE IV: Approximate branching fractions for the decay of $t\bar{t}$ through $t \rightarrow bW$.

For the computation of the amplitudes we assume the quarks u, d, s, c and the leptons e, μ to be massless. The Cabibbo-Kobayashi-Maskawa (CKM) matrix is correspondingly assumed to be diagonal. We ignore diagrams with internal Higgs boson lines, which are negligibly small. We use the proton PDF CTEQ6m, and choose the factorization and renormalization scales to be set on an event-by-event basis to $\mu_f = \sqrt{4m_t^2 + \sum_i |\vec{p}_T(i)|^2} = \mu_r$, where the sum extends to all particles in the final state. The PHP and DIS processes show a significant dependence on the scale, with the cross section decreasing the higher the scale is set [26]. Our choice of scale yields essentially the same numerical results for the cross sections as $\mu_f = \sqrt{\hat{s}} = \mu_r$, which are about 10% lower than those obtained with a fixed scale $\mu_f = 2m_t = \mu_r$. For PHP processes we use the photon distribution function resulting from

the improved Weizsäcker-Williams equivalent-photon approximation [31] as implemented in MADGRAPH [27].

A. Semileptonic mode

For the semileptonic mode the signal (S) and signal plus total irreducible background ($S + B$) in the SM are defined as

$$S : \gamma g \rightarrow t\bar{t} \rightarrow b\bar{b}jj\ell\nu, \quad S + B : \gamma g \rightarrow b\bar{b}jj\ell\nu, \quad (7)$$

with $\ell = e^\pm, \mu^\pm$ and $j = u, \bar{u}, d, \bar{d}, s, \bar{s}, c, \bar{c}$. In the SM the signal process S involves 16 Feynman diagrams, whereas $S + B$ involves 3704 diagrams in total, 2952 with one QCD vertex and five electroweak vertices like the signal process, and 752 with three QCD vertices and three electroweak vertices. Some of these are displayed in Figs. 2 and 3.

For the computation of the cross section we impose on the final-state momenta a set of appropriate phase-space cuts. We have considered several such sets defined as

$$\begin{aligned} C_0 : & |\eta(j)| < 5, \quad |\vec{p}_T(j)| > 1 \text{ GeV}, \quad |\eta(\ell)| < 5, \quad |\vec{p}_T(\ell)| > 1 \text{ GeV}, \\ C_1 : & \begin{cases} |\eta(j)| < 5, \quad |\vec{p}_T(j)| > 5 \text{ GeV}, \quad |\eta(\ell)| < 5, \quad |\vec{p}_T(\ell)| > 5 \text{ GeV}, \quad \cancel{E}_T > 5 \text{ GeV}, \\ |\eta(b)| < 3, \quad |\vec{p}_T(b)| > \begin{cases} 15 \text{ GeV} & (E_e = 60 \text{ GeV}) \\ 20 \text{ GeV} & (E_e = 140 \text{ GeV}) \end{cases} \end{cases}, \\ C_f : & C_1, \quad \Delta R(x) > 0.4 \quad (x = b\bar{b}, \ell\ell, \ell b, bj, jj), \end{aligned} \quad (8)$$

where b stands for b or \bar{b} , j refers to the light jets, ℓ to the charged leptons, and $\Delta R = \sqrt{(\Delta\eta)^2 + (\Delta\phi)^2}$ is the distance in the η - ϕ plane. The kinematic variables η, ϕ , correspond to the laboratory frame. The cuts C_0 are a minimal set needed to render the scattering amplitude for background processes free from infrared instabilities, due to the emission of massless leptons and quarks. We use C_0 only for reference. We have tested the cuts in the different kinematic variables one by one to assess their efficiency to reduce the ratio $\epsilon_\sigma = (\sigma(S + B) - \sigma(S))/\sigma(S + B)$. We have found that only the cuts in b and \bar{b} lead to a significant enhancement of the signal. In the set C_1 we use a standard centrality cut for $\eta(b)$ and choose the cut in $|\vec{p}_T(b)|$ so that $|\epsilon_\sigma| \lesssim 15\%$. The cuts on leptons and light jets do not seem effective at improving the signal-to-background ratio, so in C_1 we keep them as loose as realistically possible. Finally, in the set C_f , which is the one used in our

computations, we add standard isolation cuts for the b and light-quark jets, and the charged leptons, as idealized analogues of the ones required in actual experimental measurements. In Table V the effects of these cuts on the signal and total cross sections, computed in the SM, are summarized. Whereas a 15% background is sufficiently small for our purposes, further

	$E_e = 60 \text{ GeV}$			$E_e = 140 \text{ GeV}$		
	$\sigma(S)[\text{fb}]$	$\sigma(S+B)[\text{fb}]$	ϵ_σ	$\sigma(S)[\text{fb}]$	$\sigma(S+B)[\text{fb}]$	ϵ_σ
\emptyset	5.91			30.94		
C_0	5.84	9.21	36.6%	30.92	47.09	34.3%
C_1	4.50	5.26	14.4%	25.59	29.87	14.3%
C_f	3.85	4.50	14.4%	22.25	25.90	14.1%

TABLE V: The effect of the cuts defined in Eq. (8) on the SM signal and total semileptonic cross sections. \emptyset refers to no cuts.

enhancement of the signal is in principle possible by imposing additional cuts: for instance, on the invariant mass of the hadronic decay products. Let us assume a cut of the form

$$\left| m_t - \sqrt{(p_b + p_q + p_{q'})^2} \right| < W, \quad (9)$$

where p_b stands for the four-momentum of either one of the two b -tagged jets and $p_q, p_{q'}$ for those of the non- b jets. Then, at $E_e = 140 \text{ GeV}$ and $W = 30 \text{ GeV}$, with the cut (9) in addition to C_f , we get $\sigma(S) = 22.06 \text{ fb}$ and $\sigma(S+B) = 24.90 \text{ fb}$, corresponding to $\epsilon_\sigma = 11\%$, which constitutes a slight improvement on C_f . An even larger enhancement of the signal would be obtained in the ideal case in which the missing momentum carried by the neutrino could be fully reconstructed. In that case, imposing the cuts C_f together with Eq. (9) and the analogous cut on the leptonic decay products leads to $\sigma(S) = 21.79 \text{ fb}$ and $\sigma(S+B) = 23.30 \text{ fb}$, yielding $\epsilon_\sigma = 6 \%$, which is less than one half of the background level in Table V.

With an integrated luminosity of 100 fb^{-1} and the cross sections from Table V, at $E_e = 60 \text{ GeV}$ we expect ~ 385 photo-production events. Taking into account a b -tagging efficiency of 60% per b -jet, we are left with about 140 events corresponding to a statistical error of 8.4%. Similarly, at $E_e = 140 \text{ GeV}$ the expected statistical error is 3.5%.

One important source of systematic errors lies in the SM reducible background to the signal process S in Eq. (7), given by processes of the form $e^-(\gamma)p \rightarrow jjjj\ell\nu$ (where j stands

for a gluon or a quark or antiquark of the first two generations) or $e^-(\gamma)p \rightarrow bj\bar{j}\ell\nu$ (where b refers to b or \bar{b}). The former class of processes involves two b -mistagging, and their cross section is smaller than that of the signal by about two orders of magnitude which, multiplied by the probability of two mistagging, results in a negligible contribution. We take the b -mistagging probability to be 1/10 for c , and 1/100 for lighter partons. The second class of processes, involving a single b -mistagging, comprises 7408 Feynman diagrams. The overwhelmingly dominant contribution to the cross section, however, originates in diagrams containing two resonant intermediate propagators.

Thus, the reducible background is essentially given by the processes

$$\gamma b \rightarrow tW \rightarrow bgc\bar{s}\ell\nu \quad \text{or} \quad \gamma b \rightarrow tW \rightarrow bgu\bar{d}\ell\nu, \quad (10)$$

where the quark symbols stand for either those quarks or their antiquarks, and ℓ stands for e^\pm, μ^\pm . All possible quark and lepton flavor combinations in the final state result in 204 diagrams for the charmed process, and as many diagrams for the charmless final state, with a cross section of 10.5 fb each at $E_e = 140$ GeV, and 2.04 fb each at $E_e = 60$ GeV. We have explicitly separated the charmed and charmless final states in Eq. (10) due to the different mistagging probabilities for the c and lighter partons. For each of the processes in Eq. (10) we have to ascertain the fraction of events in which some or none of the three non- b jets pass the cuts for b -jets (so they can therefore potentially be mistagged), how many of them there are, and whether those jets passing the cuts are c or lighter. For brevity, we skip the combinatorial analysis and the results for the partial cross sections for each case and just state the results. At $E_e = 140$ GeV the cross section for events with a single b -mistagging is 1.15 fb, or 5.16% of $\sigma(S)$ as given in Table V, and at $E_e = 60$ GeV it is 0.25 fb, or 6.5% of $\sigma(S)$.

Adding the statistical and mistagging errors discussed above in quadrature we obtain an error of 10.6% at $E_e = 60$ GeV and 6.2% at $E_e = 140$ GeV. Allowing for other unspecified sources of systematical error, we consider total experimental errors of 18% and 10% at $E_e = 60$ and 140 GeV, respectively, as plausible estimates.

B. Dileptonic and hadronic modes

For the dileptonic mode the signal (S) and signal plus total irreducible background ($S+B$) in the SM are given by

$$S : \gamma g \rightarrow t\bar{t} \rightarrow b\bar{b}\ell^+\nu\ell^-\bar{\nu} \quad S + B : \gamma g \rightarrow b\bar{b}\ell^+\nu\ell^-\bar{\nu} \quad (11)$$

with $\ell = e, \mu$. The signal process S involves eight Feynman diagrams, and $S + B$ 1104 diagrams with one strong, one electromagnetic and four weak vertices as the signal diagrams.

For the computation of the cross section we impose the same cuts as those defined in Eq. (8). The effects of these cuts on the signal and total cross sections are summarized in Table VI. Assuming the same integrated luminosity and b -tagging efficiency as in the

	$E_e = 60 \text{ GeV}$			$E_e = 140 \text{ GeV}$		
	$\sigma(S)[\text{fb}]$	$\sigma(S+B)[\text{fb}]$	ϵ_σ	$\sigma(S)[\text{fb}]$	$\sigma(S+B)[\text{fb}]$	ϵ_σ
\emptyset	0.98			5.16		
C_f	0.66	0.77	14.3%	3.83	4.45	13.9%

TABLE VI: The effect of the cuts defined in Eq. (8) on the SM signal and total dileptonic-mode cross sections.

semileptonic mode leads us to an expected statistical error of 14% at $E_e = 60 \text{ GeV}$ and 6% at 140 GeV. Given that this dileptonic mode should not be affected by strong systematical errors, the total experimental uncertainties would probably not be much larger than those found for the semileptonic mode.

For the hadronic mode the signal (S) and signal plus total irreducible background ($S+B$) in the SM are given by

$$S : \gamma g \rightarrow t\bar{t} \rightarrow b\bar{b}W^+W^- \rightarrow b\bar{b}jjjj \quad S + B : \gamma g \rightarrow b\bar{b}jjjj . \quad (12)$$

The signal process S involves eight Feynman diagrams, each with one electromagnetic, one strong, and four weak vertices, and $S + B$ 50700 diagrams, 21 592 with one QCD and five electroweak vertices, 22 304 with three QCD and three electroweak vertices, and 6804 with one electromagnetic and five QCD vertices.

For the computation of the cross section we may impose the same cuts as those defined in Eq. (8). Due to the large irreducible background, however, these cuts are not enough to

achieve $\epsilon_\sigma \lesssim 15\%$. We therefore introduce in this case the more restrictive set of cuts

$$C'_f : \begin{cases} |\eta(j)| < 5, & |\vec{p}_T(j)| > 15 \text{ GeV}, & |\eta(\ell)| < 5, & |\vec{p}_T(\ell)| > 15 \text{ GeV}, & \cancel{E}_T > 10 \text{ GeV}, \\ |\eta(b)| < 3, & |\vec{p}_T(b)| > \begin{cases} 20 \text{ GeV} & (E_e = 60 \text{ GeV}) \\ 25 \text{ GeV} & (E_e = 140 \text{ GeV}) \end{cases}, \\ \Delta R(x) > 0.4 & (x = b\bar{b}, \ell\ell, \ell b, bj, jj), \end{cases} \quad (13)$$

The effects of these cuts on the signal and total cross sections are summarized in Table VII. The values of the cross section after cuts are virtually the same as in the semileptonic case.

	$E_e = 60 \text{ GeV}$			$E_e = 140 \text{ GeV}$		
	$\sigma(S)$ [fb]	$\sigma(S + B)$ [fb]	ϵ_σ	$\sigma(S)$ [fb]	$\sigma(S + B)$ [fb]	ϵ_σ
\emptyset	8.84			46.40		
C_f	5.63	12.82	56%	32.56	50.38	35%
C'_f	4.13	4.80	14%	23.33	26.81	13%

TABLE VII: The effect of the cuts defined in Eq. (8) and (13) on the SM signal and total hadronic-mode cross sections.

Therefore, the statistical errors will also be the same, but the systematical errors for this mode are expected to be significantly higher.

C. Contribution from the effective operators

For the computation of the amplitudes in the effective theory we make the same approximations—i.e., the first two generations are massless and the CKM matrix is diagonal—as in the SM calculations of the previous sections. We also make the same choice of PDF and of factorization and renormalization scales. We implemented the basis of dimension-six $SU(2) \times U(1)$ -invariant effective operators described above in MADGRAPH 5 [27] by means of the program FEYNRULES 1.6 [32] (see also Ref. [33] for a more recent description).

We have explicitly checked that the bounds obtained on the effective couplings are essentially independent of the choice of energy ($E_e = 60, 140$, or even 300 GeV) and of production mode (dileptonic, semileptonic, or hadronic), provided the signal-to-background ratio and the assumed experimental error are kept fixed. For this reason we present results for two

possible error values: 18% (as estimated for $E_e = 60$ GeV in Sec. IV A) and 10% (as estimated for $E_e = 140$ GeV). We computed the results given below for the semileptonic mode of photo-production, with the set of cuts C_f defined in Eq. (8), whose cross section is significantly larger than that of the dileptonic mode, and whose background is significantly smaller than that of the hadronic mode.

For photo-production only two operators contribute to the amplitude: $O_{uW\phi}^{33}$ and $O_{uB\phi}^{33}$ (we disregard $O_{uG\phi}^{33}$, to which the sensitivity at the LHC is much higher). In addition to the SM diagrams, other diagrams are computed that contain the contribution from $O_{uW\phi}^{33}$ as well as the contribution from $O_{uB\phi}^{33}$ (see Fig. 2). Notice that the diagrams with two effective vertices in Fig. 2 must be kept in the amplitude since, through their interference with the SM diagrams, they make contributions of second order in the effective couplings to the cross section. In fact, due to the fact that $O_{uW\phi}^{33}$ contains both charged- and neutral-current vertices, tree-level diagrams with three anomalous vertices are also possible, making third-order contributions to the amplitude $\propto C_{tB}C_{tW}^2$ and C_{tW}^3 . We have kept these contributions in our calculation. But we have explicitly verified in all cases that, for values of the effective couplings within the bounds given below, the contribution to the cross section from terms of order higher than the second is actually negligible.

	$E_e = 60$ GeV	$E_e = 140$ GeV
C_{tW}^r	$a = -0.41, b = 0.074$	$a = -0.39, b = 0.079$
C_{tW}^i	$a = 0, b = 0.10$	$a = 0, b = 0.11$
C_{tB}^r	$a = -0.74, b = 0.26$	$a = -0.72, b = 0.28$
C_{tB}^i	$a = 0, b = 0.26$	$a = 0, b = 0.28$

TABLE VIII: The a and b numbers as defined in Eq. (5) for photo-production of $t\bar{t}$ analyzed in the semileptonic channel. The corresponding numbers for the dileptonic and the hadronic channels are almost equal.

In Table VIII we show the a and b numbers as defined in Eq. (5). The corresponding numbers for the other channels are almost the same: this is because the cuts imposed on each mode affect both the SM and the anomalous contributions equally. Notice that a and b change very little when going from $E_e = 60$ GeV to $E_e = 140$ GeV. In Table IX we show the limits on C_{tW} and C_{tB} for experimental uncertainties $\epsilon = 10\%$ and $\epsilon = 18\%$, where we

$\epsilon = 10\%$	min	max	$\epsilon = 18\%$	min	max
C_{tW}^r	-0.24	0.27	C_{tW}^r	-0.42	0.51
C_{tW}^i	-0.97	0.97	C_{tW}^i	-1.30	1.30
C_{tB}^r	-0.13	0.15	C_{tB}^r	-0.23	0.28
C_{tB}^i	-0.60	0.60	C_{tB}^i	-0.81	0.81

TABLE IX: The bounds obtained from the contribution to $t\bar{t}$ photo-production taking one operator at a time.

take only one coefficient to be nonzero at a time. Notice that the bounds given in the table are essentially equal to those found in Sec. III from a simpler analysis at the level of $t\bar{t}$. This is due to the fact that $O_{uB\phi}^{33}$ only enters the $t\bar{t}\gamma$ production vertex, whereas O_{uW}^{33} also enters the decay vertex. However, because of the tensor character of its coupling the dominant contribution of O_{uW}^{33} comes from the production vertex as well. Notice also that the bounds on C_{tB} shown in Table IX are substantially stronger than those in Table II. The bounds on C_{tW} will also be stronger at the LHeC, although in that case the largest sensitivity will be achieved at the LHC14 and at the LHeC in the single top channel [2].

In general, there are correlations and mixed terms in Eq. (5). This is due to the interference between amplitudes of the same CP nature. In fact, to the R ratio in Eq. (5) we can add

$$R \rightarrow R + 0.3C_{tW}^r C_{tB}^r + 0.3C_{tW}^i C_{tB}^i \quad (14)$$

in order to keep track of the correlation. In Fig. 4 we show different allowed parameter regions taking two couplings at a time. The regions in Fig. 4(a) and 4(c) would be significantly reduced once the stricter bounds on C_{tW}^r from single top production are included [2]. For values of C_{tW} and C_{tB} as small as those given in Table IX or in Fig. 4, the PHP cross section depends on those effective couplings essentially only through the MDM κ and the EDM $\tilde{\kappa}$ as defined in Eq. (3), as can be seen in Figs. 4(c) and 4(d). In Fig. 5 we show the correlated bounds between κ and $\tilde{\kappa}$. Notice the great reduction from the presently known allowed parameter region, even if we include a potential bounded region coming from $t\bar{t}\gamma$ production at the LHC[19].

The SM prediction for a_t [Eq. (4)] is $a_t^{\text{SM}} = 0.02$ [34], which translates to $\kappa^{\text{SM}} = 0.013$. On the other hand, the CP-violating EDM factor d_t is strongly suppressed in the SM:

$d_t^{\text{SM}} < 10^{-30} e \text{ cm}$ ($\tilde{\kappa} < 1.75 \times 10^{-14}$)[35]. These predictions are too small to be probed at the LHeC. Notice the bounds of order 0.05 for κ and 0.2 for $\tilde{\kappa}$ as shown in Fig. 5. Of course, the prediction for the MDM is really not so far from the sensitivity of the LHeC at the planned energies. The EDM value in the SM is so suppressed that it could be a very good probe of new physics[36]. There are models with vector-like multiplets that predict values as high as $10^{-19} e \text{ cm}$ ($\tilde{\kappa} < 1.75 \times 10^{-3}$) [3]. In fact, these models can also predict large values of other CP-odd top-quark properties like the chromoelectric dipole moment [4]. As with the SM value for κ , these new physics predictions of $\tilde{\kappa}$ are not too far from the LHeC sensitivity.

Figures 4(c) and 4(d) can be expressed in terms of the top magnetic dipole moments κ and κ_Z and their electric counterparts. We do so below in Sec. V, where we also incorporate bounds from $t\bar{t}$ production in DIS.

D. Effects of irreducible background

In order to assess more accurately the effects on our results of the irreducible background processes passing the cuts, we repeated a small part of the analysis of the previous section including background effects. We considered only the semileptonic mode in PHP, $e^-(\gamma)p(g) \rightarrow b\bar{b}j\ell\nu$, including all possible insertions of the anomalous operators $O_{uW\phi}^{33}$ and $O_{uB\phi}^{33}$. The resulting amplitude consists of 5136 Feynman diagrams, excluding those with internal Higgs lines, as was done for the calculation with the signal process. The results obtained considering one coupling at a time are displayed in Table X. The bounds on C_{tW} and C_{tB} shown there are about 15% weaker than those in Table IX from the signal process only, in line with our expectations from the more limited analysis of the SM irreducible background in Sec. IV A.

V. LIMITS FROM DIS PRODUCTION OF $t\bar{t}$

The cross section for $t\bar{t}$ production in DIS will be somewhat lower than that of PHP. Thus, the bounds from DIS on C_{tW} and C_{tB} will be correspondingly weaker than those from PHP. But they will also be complementary. First, since the DIS process probes the $t\bar{t}Z$ vertex it can be used to set constraints on the $t_R t_R Z$ coupling $C_{\phi t}$. Second, because the dependence of the DIS and PHP cross sections on C_{tW} and C_{tB} are different, the allowed

$\epsilon = 10\%$	min	max	$\epsilon = 18\%$	min	max
C_{tW}^r	-0.28	0.32	C_{tW}^r	-0.48	0.62
C_{tW}^i	-1.02	1.02	C_{tW}^i	-1.37	1.37
C_{tB}^r	-0.15	0.17	C_{tB}^r	-0.26	0.33
C_{tB}^i	-0.65	0.65	C_{tB}^i	-0.87	0.87

TABLE X: The bounds obtained from $t\bar{t}$ photo-production including irreducible background, with the set of cuts C_f from Eq. (8).

regions on the planes $C_{tW}^r-C_{tB}^r$ and $C_{tW}^i-C_{tB}^i$ are given by the intersection of the regions allowed by each process.

As in the case of $t\bar{t}$ PHP, the three production modes lead to the same results, for fixed signal-to-background ratios and experimental uncertainties. For brevity we restrict ourselves here to the semileptonic mode, whose cross section is larger than that of the dileptonic mode and whose background is simpler than that of the hadronic mode. We use for DIS the same global parameter values and the same set of cuts C_f defined by Eq. (8) for the case of photo-production. The signal and total processes in this case are, with the same notation as in Eq. (7),

$$S : e^-p(g) \rightarrow e^-t\bar{t} \rightarrow e^-b\bar{b}jj\ell\nu, \quad S + B : e^-p(g) \rightarrow e^-b\bar{b}jj\ell\nu. \quad (15)$$

The amplitude for the signal process S involves 40 Feynman diagrams and $S + B$ involves 14844 diagrams, where we have ignored diagrams with internal Higgs lines whose contribution is numerically negligible. At $E_e = 60$ GeV we have $\sigma(S) = 2.2$ fb, $\sigma(S + B) = 2.3$ fb, and $\epsilon_\sigma = 4.3\%$, and at $E_e = 140$ GeV we have $\sigma(S) = 15.8$ fb, $\sigma(S + B) = 14.7$ fb, and $\epsilon_\sigma = -7\%$. Notice that at 140 GeV there is destructive interference between signal and irreducible background. Given these SM cross sections, and assuming an integrated luminosity of 100 fb^{-1} and a b -tagging efficiency of 60%, the statistical errors are estimated to be 11% and 4% at $E_e = 60$ and 140 GeV, respectively. With these statistical errors we consider it reasonable to stick to the same estimates of total experimental uncertainties in the range 10%–18% as in PHP.

At LHeC-energy scattering events are considered to be in the DIS regime if $|Q_\gamma^2| > 2 \text{ GeV}^2$ [1]. Since we do not apply this cut on Q_γ^2 directly, it is necessary to verify that our cuts C_f ensure that it is satisfied. This is clearly seen in Fig. 6, where the Q_γ^2 distribution

has a lower end point at $|Q_\gamma^2| \gtrsim 30 \text{ GeV}^2$.

For the expression of R Eq. (5) we show the a and b numbers in Table XI. We also add

	$C_{\phi t}^r$	C_{tW}^r	C_{tW}^i	C_{tB}^r	C_{tB}^i
a	-0.015	-0.24	0	-0.40	0
b	2.5×10^{-4}	0.062	0.085	0.16	0.17

TABLE XI: The a and b numbers as defined in Eq. (5) for DIS production of $t\bar{t}$ analyzed in the semileptonic channel. The corresponding numbers for the dileptonic and the hadronic channels are almost equal.

the terms

$$R \rightarrow R + 0.17C_{tW}^r C_{tB}^r + 0.17C_{tW}^i C_{tB}^i \quad (16)$$

in order to obtain the correlation between different parameters. There is a $+10^{-5}C_{tB}^r C_{\phi t}$ term that we consider to be negligible. In Fig. 7 we show the correlated allowed parameter region for C_{tB}^r and $C_{\phi t}$. As seen in the figure, the bounds that the LHeC will be able to set on the $t_R t_R Z$ coupling will not be very stringent. The allowed regions for C_{tW}^r vs C_{tB}^r and C_{tW}^i vs C_{tB}^i can be transformed into plots for κ vs κ_Z and $\tilde{\kappa}$ vs $\tilde{\kappa}_Z$. In Fig. 8 we show the allowed parameter region including also the constraints from photo-production. The direct bounds on κ_Z that would be obtained, $-1 < \kappa_Z < 1.4$ with an experimental error of $\epsilon = 18\%$ and $-0.7 < \kappa_Z < 1.1$ with 10% , are somewhat weaker than the analogous ones obtained from the indirect bounds on C_{tW}^r, C_{tB}^r from Table II. On the other hand, to our knowledge, there are no bounds on $\tilde{\kappa}_Z$ in the literature. From Fig. 8 we get $|\tilde{\kappa}_Z| < 0.78$ at $\epsilon = 18\%$ and $|\tilde{\kappa}_Z| < 0.59$ at $\epsilon = 10\%$.

VI. FINAL REMARKS

In this paper we have investigated the sensitivity of the LHeC to probe top-quark effective couplings with the gauge bosons. We have chosen the set of eight gauge-invariant dimension-six operators to describe the anomalous couplings of top and gauge bosons (gluon, photon, and weak bosons). Two operator coefficients have been related ($C_{\phi q}^{(3,33)} = -C_{\phi q}^{(1,33)} \equiv C_{\phi q}$) so that the $b_L b_L Z$ effective coupling retains its SM value. In addition, the anomalous top-gluon

coupling already has strong direct constraints from LHC data. Indeed, the LHC 14 TeV run will reach a much larger sensitivity than what the LHeC would for this coupling, so we do not include it in our study. Therefore, we have six independent coefficients— $C_{\phi q}$, $C_{\phi\phi}$, $C_{\phi t}$, C_{bW} , C_{tW} , and C_{tB} —that can be probed at the LHeC through the three largest production modes. These are 1) single (anti)top, 2) $t\bar{t}$, and 3) top and W associated production.

Concerning single antitop production, in Ref. [2] it has been shown that the LHeC could probe the effective tbW couplings with a sensitivity that is much better than that achievable at the LHC. As is well known, the anomalous tbW couplings can change the W -boson helicity in top decay process [21]. Consequently, various kinematical asymmetries of the top decay products that directly depend on the W helicity were considered in Ref. [2]. Assuming an uncertainty of 2% in the experimental measurements, they obtained constraints that are approximately as follows: $-0.05 < C_{\phi q} < 0.05$, $-1.6 < C_{\phi\phi}^r < 2.6$, $-0.04 < C_{tW}^r < 0.04$ and $-0.4 < C_{bW}^r < 0.8$. Notice that the constraints on $C_{\phi\phi}^r$ and C_{bW}^r are much weaker. This is because these operators are related to right-handed bottom quarks and there is a negligible interference with the SM amplitude. On the other hand, if we assume that the single top cross section is measured with the 2% (essentially systematic) error that is assumed for the asymmetries in Ref. [2], we obtain (based only on the cross section) $-0.34 < C_{\phi q} < 0.33$, $|C_{\phi\phi}| < 2.8$, $-0.7 < C_{tW}^r < 0.9$, and $|C_{bW}^r| < 1.1$. The bounds for $C_{\phi q}$ and C_{tW}^r obtained from the variation of $\sigma(ep \rightarrow \nu\bar{t})$ are about one order of magnitude weaker than the bounds obtained by analyzing the W -boson helicity in the decay of \bar{t} . On the other hand, the bounds for $C_{\phi\phi}^r$ and C_{bW}^r (that involve b_R) are of about the same order of magnitude.

As for top and W associated production, with about 0.031 pb at $E_e = 60$ GeV this mode could somewhat help in probing the tbW coupling. There is no specific study on the sensitivity for this process at the LHeC, but rather only for the case of an LHeC-based γp collider where the enhanced emission of very energetic photons from the initial $E_e = 60$ GeV electron beam can reach a cross section $\sigma(tW^-) = 0.5$ pb [37].

Our focus is on the potential to probe the MDM and the EDM of the top quark through the $t\bar{t}$ photo-production process. The sensitivity changes very little when going from $E_e = 60$ GeV to $E_e = 140$ GeV: it only depends on the accuracy achieved in measuring the production cross section, which can be much better at 140 GeV due to the larger event sample. We assumed two possible values of the experimental error $\Delta\sigma/\sigma = 10\%$, 18% and derived allowed regions for the MDM $\kappa = 2m_t\mu_t/e$ and the EDM $\tilde{\kappa} = 2m_t d_t/e$ as shown in Fig. 5. In both

cases, the measurement of the $t\bar{t}$ photo-production at the LHeC could greatly improve the limits imposed by the indirect constraints from $b \rightarrow s\gamma$ and even the limits imposed by a future measurement of $t\bar{t}\gamma$ production at the LHC (14 TeV). Specifically, measuring $\sigma(\gamma e \rightarrow t\bar{t})$ with 10% (18%) error would yield the bounds $|\kappa| < 0.05$ (0.09) and $|\tilde{\kappa}| < 0.20$ (0.28). We have also considered the DIS production mode of $t\bar{t}$ which is somewhat smaller than photo-production. In this case there is a sensitivity to ttZ couplings as well. However, this sensitivity is rather weak: the bounds on the $t_R t_R Z$ coupling would be $-6.2(-10.3) < C_{\phi t} < 7.5(14.8)$ which are weaker than the current indirect limits $-0.1 < C_{\phi t} < 3.7$.

Acknowledgments We gratefully thank O. Mattelaer and J. Alwall for their helpful information on MADGRAPH 5. This work has been partially supported by Sistema Nacional de Investigadores de México.

-
- [1] J. L. Abelleira Fernandez *et al.* [LHeC Study Group Collaboration], J. Phys. G **39**, 075001 (2012). See [arXiv:1206.2913v2 [physics.acc-ph]].
- [2] S. Dutta, A. Goyal, M. Kumar and B. Mellado, arXiv:1307.1688 [hep-ph].
- [3] T. Ibrahim and P. Nath, Phys. Rev. D **82**, 055001 (2010).
- [4] T. Ibrahim, P. Nath and , Phys. Rev. D **84**, 015003 (2011).
- [5] F. Penunuri and F. Larios, Phys. Rev. D **79**, 015013 (2009) [arXiv:0810.4545 [hep-ph]]; A. Belyaev, C. -R. Chen, K. Tobe and C. -P. Yuan, Phys. Rev. D **74**, 115020 (2006) [hep-ph/0609179]; Q. -H. Cao, C. -R. Chen, F. Larios and C. -P. Yuan, Phys. Rev. D **79**, 015004 (2009) [arXiv:0801.2998 [hep-ph]]; C. F. Berger, M. Perelstein and F. Petriello, hep-ph/0512053.
- [6] R. S. Chivukula, P. Ittisamai, E. H. Simmons, B. Coleppa, H. E. Logan, A. Martin and J. Ren, Phys. Rev. D **86**, 095017 (2012) [arXiv:1207.0450 [hep-ph]]; E. H. Simmons, A. Atre, R. S. Chivukula, P. Ittisamai, N. Vignaroli, A. Farzinnia and R. Foadi, arXiv:1304.0255 [hep-ph]; R. S. Chivukula, E. H. Simmons and N. Vignaroli, Phys. Rev. D **87**, 075002 (2013) [arXiv:1302.1069 [hep-ph]]; E. H. Simmons, R. S. Chivukula, B. Coleppa, H. E. Logan and A. Martin, arXiv:1112.3538 [hep-ph]; C. -X. Yue, J. Guo, J. Zhang and Q. -G. Zeng, Commun. Theor. Phys. **58**, 711 (2012) [arXiv:1203.3627 [hep-ph]].
- [7] X. -F. Wang, C. Du and H. -J. He, Phys. Lett. B **723**, 314 (2013) [arXiv:1304.2257 [hep-ph]];

- H. -J. He, T. M. P. Tait and C. P. Yuan, Phys. Rev. D **62**, 011702 (2000) [hep-ph/9911266].
- [8] K. Kumar, T. M. P. Tait and R. Vega-Morales, JHEP **0905**, 022 (2009) [arXiv:0901.3808 [hep-ph]]; B. Lillie, J. Shu and T. M. P. Tait, JHEP **0804**, 087 (2008) [arXiv:0712.3057 [hep-ph]]; N. Zhou, D. Whiteson and T. M. P. Tait, Phys. Rev. D **85**, 091501 (2012) [arXiv:1203.5862 [hep-ph]]; R. S. Chivukula, R. Foadi and E. H. Simmons, Phys. Rev. D **84**, 035026 (2011) [arXiv:1105.5437 [hep-ph]].
- [9] W. Buchmueller and D. Wyler, Nucl. Phys. B **268** (1986) 621.
- [10] B. Grzadkowski, Z. Hioki, K. Ohkuma, J. Wudka, Nucl. Phys. B **689**, 108 (2004).
- [11] J. A. Aguilar-Saavedra, Nucl. Phys. B **812** (2009) 181.
- [12] B. Grzadkowski, M. Iskrzynski, M. Misiak, J. Rosiek, JHEP **1010**, 085 (2010).
- [13] M. Einhorn and J. Wudka, arXiv:1307.0478 [hep-ph].
- [14] I. T. Cakir, O. Cakir and S. Sultansoy, Phys. Lett. B **685**, 170 (2010)
- [15] J. A. Aguilar-Saavedra, Nucl. Phys. B **821** (2009) 215.
- [16] C. Zhang, N. Greiner, S. Willenbrock, Phys. Rev. D **86**, 014024 (2012).
- [17] J. A. Aguilar-Saavedra, M. C. N. Fiolhais, A. Onofre, JHEP **1207**, 180 (2012).
- [18] J. Drobnak, S. Fajfer and J. F. Kamenik, Nucl. Phys. B **855**, 82 (2012).
- [19] A. O. Bouzas and F. Larios, Phys. Rev. D **87**, 074015 (2013).
- [20] R. Martinez, M. A. Perez and N. Poveda, Eur. Phys. J. C **53**, 221 (2008).
- [21] C. -R. Chen, F. Larios and C. -P. Yuan, Phys. Lett. B **631**, 126 (2005); J. A. Aguilar-Saavedra, N. F. Castro and A. Onofre, Phys. Rev. D **83**, 117301 (2011); J. A. Aguilar-Saavedra and J. Bernabeu, Nucl. Phys. B **840**, 349 (2010).
- [22] F. -P. Schilling, Int. J. Mod. Phys. A **27**, 1230016 (2012).
- [23] Z. Hioki and K. Ohkuma, arXiv:1306.5387 [hep-ph].
- [24] J. F. Kamenik, M. Papucci and A. Weiler, Phys. Rev. D **85**, 071501 (2012); R. Martinez and J. A. Rodriguez, Phys. Rev. D **55**, 3212 (1997).
- [25] U. Baur, A. Juste, L. H. Orr and D. Rainwater, Phys. Rev. D **71**, 054013 (2005); Nucl. Phys. Proc. Suppl. **160**, 17 (2006). See also, M. Fael and T. Gehrmann, Phys. Rev. D **88**, 033003 (2013).
- [26] S. Moretti and K. Odagiri, Phys. Rev. D **57**, 3040 (1998).
- [27] J. Alwall, M. Herquet, F. Maltoni, O. Mattelaer, T. Stelzer, J. High Energy Phys. **06**, 128 (2011).

- [28] P. M. Nadolsky, H. -L. Lai, Q. -H. Cao, J. Huston, J. Pumplin, D. Stump, W. -K. Tung and C. -P. Yuan, Phys. Rev. D **78**, 013004 (2008).
- [29] A. Belyaev, N. D. Christensen and A. Pukhov, Comput. Phys. Commun. **184**, 1729 (2013) [arXiv:1207.6082 [hep-ph]].
- [30] J. Beringer *et al.*, Particle Data Group, Phys. Rev. D **86**, 1 (2012).
- [31] V. M. Budnev, I. F. Ginzburg, G. V. Meledin, V. G. Serbo, Phys. Rep. **15C** (1975) 181.
- [32] N. D. Christensen, C. Duhr, Comput. Phys. Commun. **180**, 1614 (2009).
- [33] S. Ask *et al.*, arXiv:1209.0297.
- [34] W. Bernreuther, R. Bonciani, T. Gehrmann, R. Heinesch, T. Leineweber, P. Mastrolia, E. Remiddi, Phys. Rev. Lett. **95**, 261802 (2005).
- [35] A. Soni and R. M. Xu, Phys. Rev. Lett. **69**, 33 (1992); F. Hoogeveen, Nucl. Phys. B341, 322 (1990); M. E. Pospelov and I. B. Khriplovich, Yad. Fiz. **53**, 1030 (1991) [Sov. J. Nucl. Phys. **53**, 638 (1991)].
- [36] D. Atwood, S. Bar-Shalom, G. Eilam and A. Soni, Phys. Rept. **347**, 1 (2001); T. Ibrahim and P. Nath, Rev. Mod. Phys. **80**, 577 (2008).
- [37] I. T. Cakir, A. Senol and A. T. Tasci, arXiv:1301.2617 [hep-ph].
- [38] The covariant derivatives as well as the non-abelian part of the tensor gauge fields are defined with the opposite sign in [11]
- [39] A study based on the FC operators (with $ij = 13, 31, 23, 32$ in (1)) would also be of great interest. For instance, in Ref. [14] the anomalous single top production at the LHeC-based γp collider is shown to have great sensitivity to the FC $tq\gamma$ vertex.

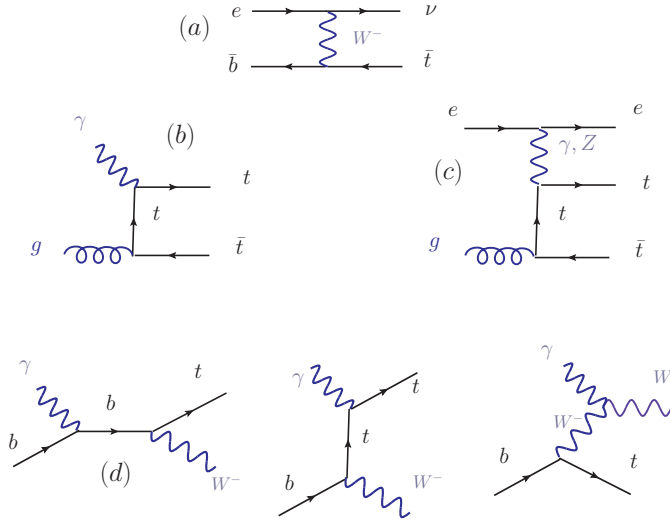


FIG. 1: The dominant top-quark production processes at the LHeC: (a) single top production, (b) $t\bar{t}$ photo-production, (c) $t\bar{t}$ DIS production, and (d) tW^- photo-production.

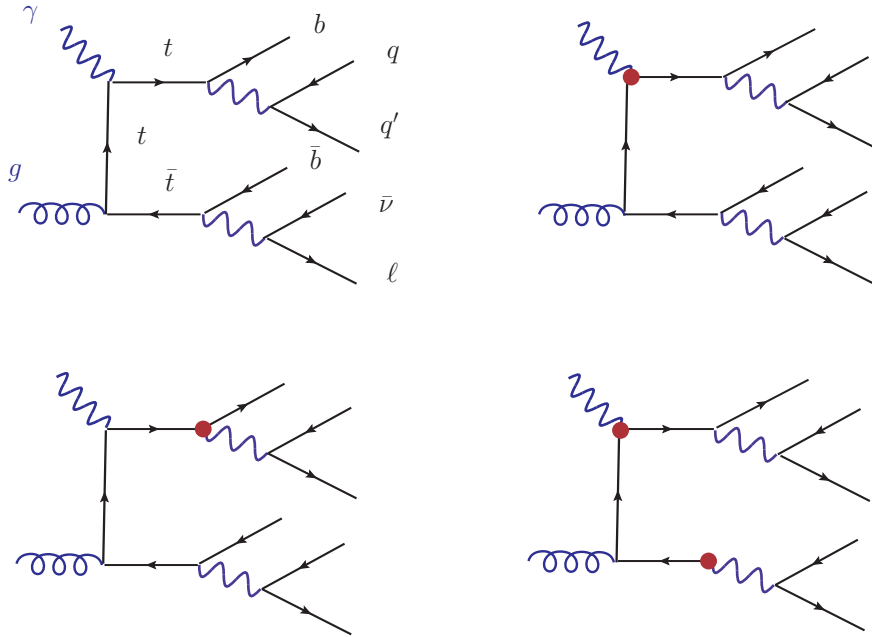


FIG. 2: The semileptonic mode for the photo-production of $t\bar{t}$ in the SM and the contribution from the effective operators. The dots indicate the presence of the anomalous couplings with contributions linear and quadratic in the coefficients C_{tW}^r and C_{tB}^r .

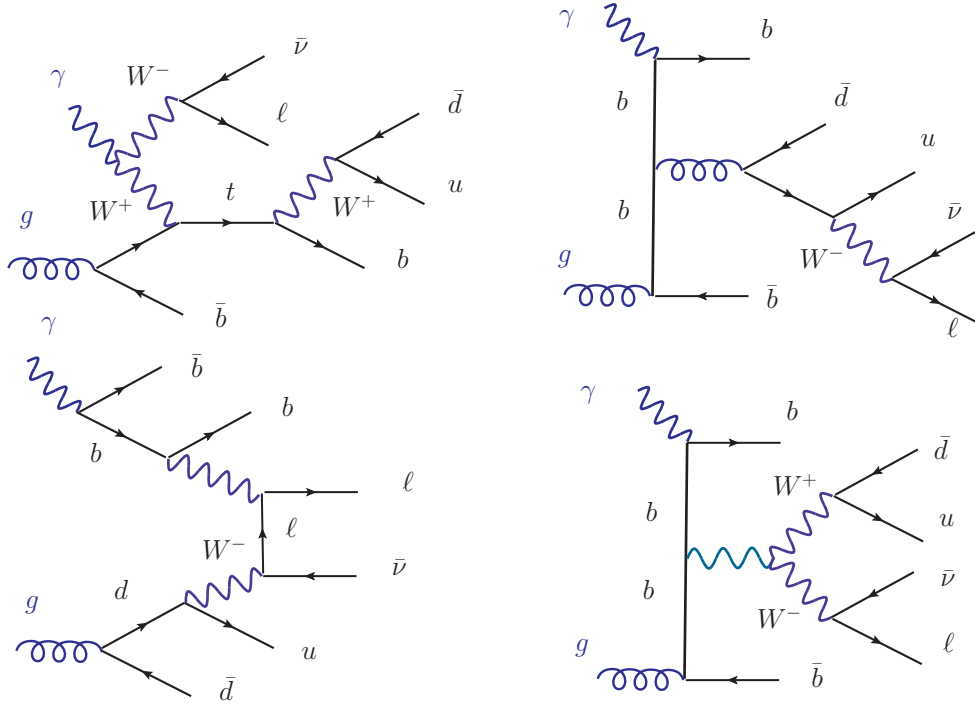


FIG. 3: Sample diagrams from the irreducible background to the semileptonic mode for the photoproduction of $t\bar{t}$ in the SM

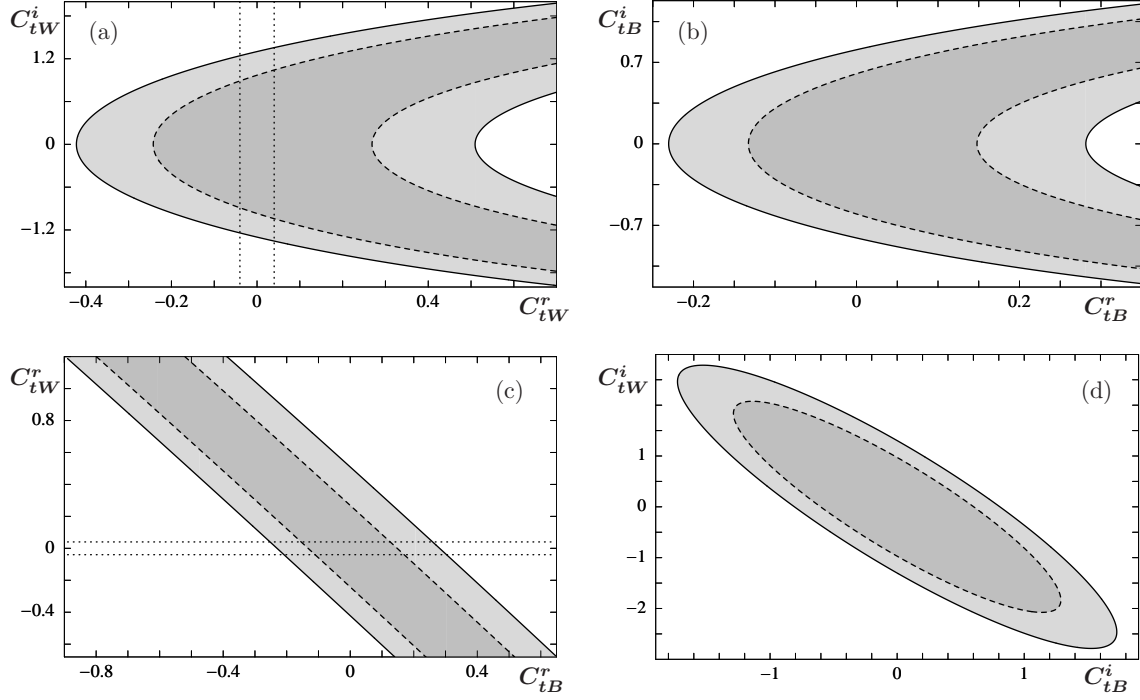


FIG. 4: Allowed regions for the effective couplings C_{tB} and C_{tW} , determined by the cross section for the semileptonic mode of $t\bar{t}$ photo-production with the cuts C_f [Eq. (8)] and assuming an experimental error of 18% (solid lines) or 10% (dashed lines). The dotted lines in (a) and (c) show the bounds on C_{tW}^r obtained in Ref. [2] from single top production and decay at the LHeC at $E_e = 60$ GeV.

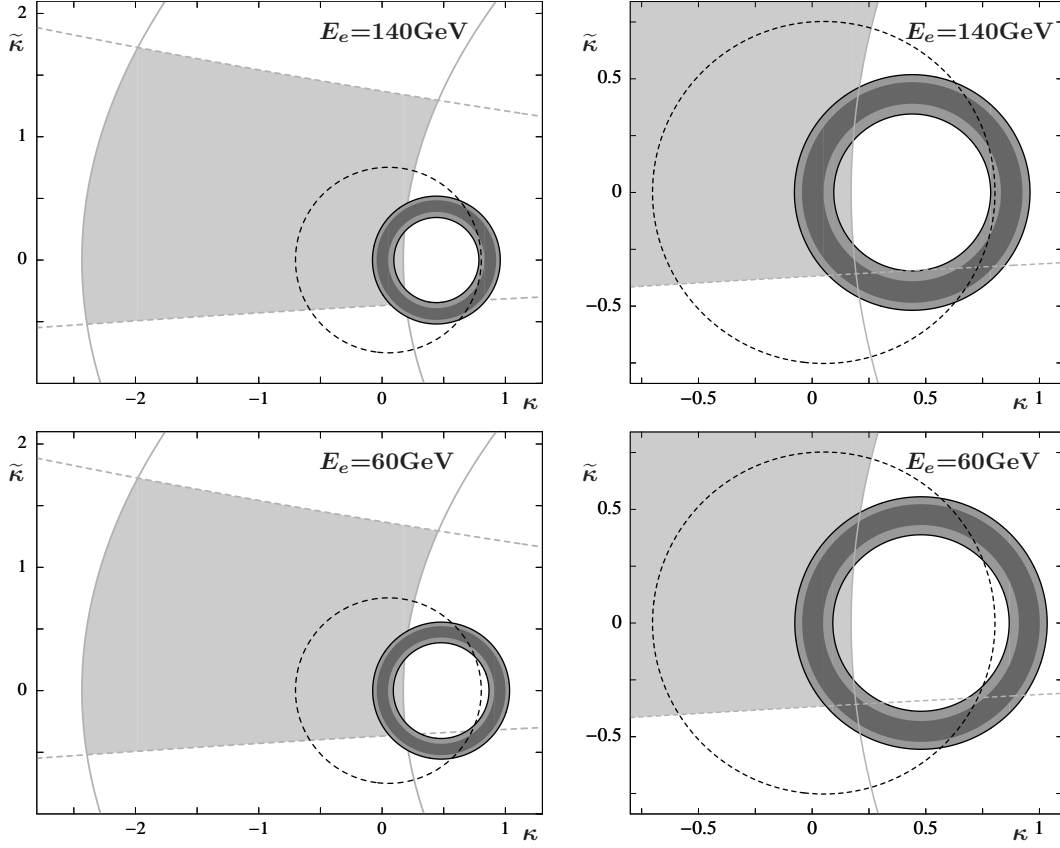


FIG. 5: Bounds on the top-quark dipole moments κ and $\tilde{\kappa}$. Light gray area: region allowed by the measurements of the branching ratio and CP asymmetry of $B \rightarrow X_s \gamma$ [19]. Dashed line: region allowed by a hypothetical experimental result for $\sigma(pp \rightarrow t\bar{t}\gamma)$ with semileptonic final state at the LHC at $\sqrt{s} = 14$ TeV with $E_T^\gamma > 10$ GeV and 5% experimental uncertainty. Solid line: region allowed by a hypothetical measurement of $\sigma(\gamma p \rightarrow t\bar{t})$ with semileptonic final state, with the cuts C_f [Eq. (8)] and 18% experimental uncertainty. Dark gray area: same as previous, with 10% experimental error.

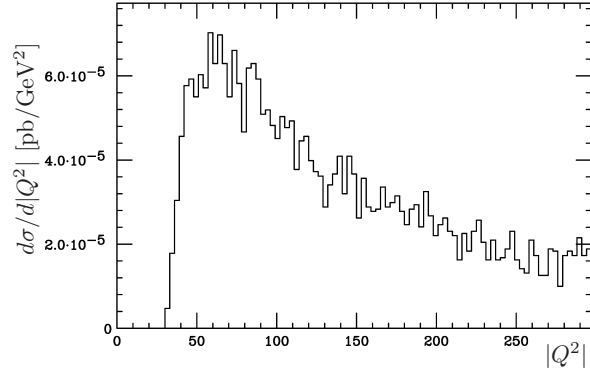


FIG. 6: Distribution of Q^2 for the process $ep \rightarrow e t \bar{t} \rightarrow ebW^+ \bar{b}W^- \rightarrow \dots$. The selection cuts C_f [Eq. (8)] ensure that the process is well into the DIS regime.

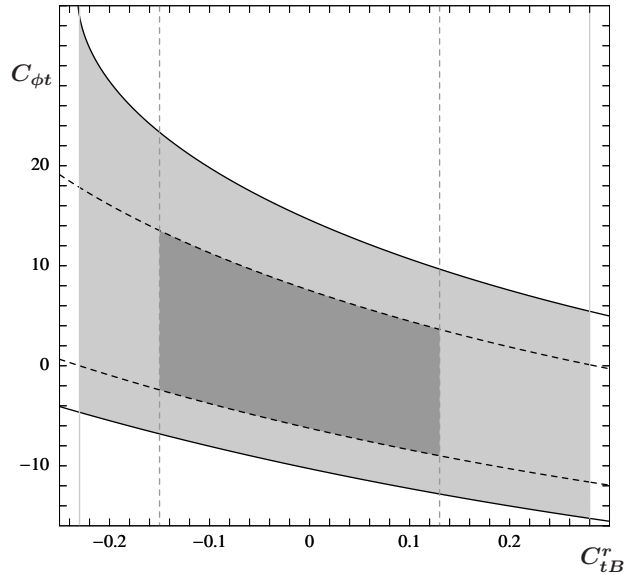


FIG. 7: Allowed region in the plane C_{tB}^r vs $C_{\phi t}$. Black lines: region allowed by DIS production of $t\bar{t}$ in the semileptonic mode with the cuts C_f [Eq. (8)] and an experimental error of 18% (solid lines) and 10% (dashed lines). Gray lines: bounds on C_{tB}^r from photo-production of $t\bar{t}$ with the same experimental errors as in DIS.

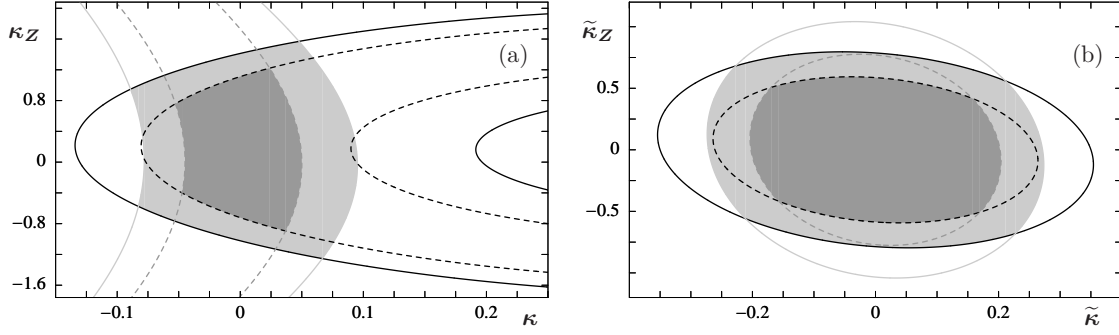


FIG. 8: Allowed regions (a) in the κ - κ_Z and (b) in the $\tilde{\kappa}$ - $\tilde{\kappa}_Z$ planes. Gray lines: areas allowed by semileptonic photo-production of $t\bar{t}$ with the cuts C_f [Eq. (8)] and an experimental error of 18% (solid line) or 10% (dashed line). Black lines: area allowed by DIS production of $t\bar{t}$ in the semileptonic mode, assuming the same values for the experimental error and with the same cuts as in photo-production.